Estimation of Flow Turbulence Metrics With a Lateral Line Probe and Regression

Ke Chen, Jeffrey A. Tuhtan, Juan Fran Fuentes-Pérez, Gert Toming, Mark Musall, Nataliya Strokina, Joni-Kristian Kämäräinen, and Maarja Kruusmaa

***Abstract*—The time-average velocity of water flow is the most commonly measured metric for both laboratory and field applications. Its employment in scientific and engineering studies often leads to an oversimplification of the underlying flow physics. In reality, complex flows are ubiquitous, and commonly arise from fluid-body interactions with man-made structures such as bridges as well as from natural flows along rocky river beds. Studying flows outside of laboratory conditions requires more detailed information in addition to time-averaged flow properties. The choice of insitu measuring device capable of delivering turbulence metrics is determined based on site accessibility, the required measuring period and overall flow complexity. Current devices are suitable for measuring turbulence under controlled laboratory conditions, and thus there remains a technology gap for turbulence measurement in the field. In this paper we show how a bio-inspired fish-shaped probe outfitted with an artificial lateral line can be utilized to measure turbulence metrics under challenging conditions. The device and proposed signal processing methods are experimentally validated in a scale vertical slot fishway, which represents an extreme turbulent environment such as those commonly encountered in the field. Optimal performance is achieved after 10 seconds of sampling using a standard deviation feature.**

***Index Terms*—bio-inspired flow sensing, artificial lateral line, turbulence, turbulence intensity, regression analysis**

I. Introduction

The research leading to these results has received funding from BONUS, the joint Baltic research and development programme, cofinanced by the European Union's Seventh Framework Programme (20072013) under the BONUS Implementation Agreement. National funding for this work has been provided by the Academy of Finland (under the grant 280715), the German Federal Ministry for Education and Research (BMBF FKZ:03F0687A), and the Estonian Environmental Investment Centre (KIK P.7254 C.3255).

K. Chen, N. Strokina and J.-K. Kämäräinen are with the Department of Signal Processing, Tampere University of Technology, Finland, e-mail: firstname.lastname@tut.fi.

J. Tuhtan, J. F. Fuentes-Pérez, G. Toming, and M. Kruusmaa are with the Center of Biorobotics, Tallinn University of Technology, Estonia.

J. Tuhtan is also with SJE Ecohydraulic Engineering GmbH.

M. Musall is with the Institute of Water and River Basin Management, Karlsruhe Institute of Technology, Germany.

TURBULENCE is the chaotic motion of fluid caused by the interaction of tangled vortices. Currently it is only possible to study turbulence in its entirety for simple flow geometries such as the flow over a step using computational fluid dynamics or particle image velocimetry (PIV). Consequently, for many applications of practical importance such as the flow of a river around a bridge pier, simplified metrics describing the bulk turbulence in terms of the fluctuations from a steady time-averaged flow have been developed and are commonly used for scientific and engineering studies of natural flows. The practical application of turbulence metrics such as the turbulence intensity require a minimum accuracy of 50% for field applications. Although standard time-averaged turbulence metrics are well-known in hydromechanics and aerodynamics communities [1], and have been validated in numerous laboratory experiments, there remains a technology gap allowing for the direct measurement of bulk turbulence in the field.

The relation between the turbulent velocity and pressure fields requires the application of a pressure Poisson equation [2]:

$$\nabla^2 P = -\rho \cdot (V \cdot \nabla V) + \nabla \cdot \frac{\partial}{\partial x_j}(\overline{u_i' u_j'}) \quad (1)$$

where P is the pressure, V is the time-averaged velocity, x_j is the spatial coordinate in the jth direction, and u' is the velocity fluctuation from the time-averaged mean. Note that $\overline{u_i' u_j'}$ is the Reynolds stress tensor, one of the parameters which is directly estimated by the proposed method.

This equation relates the velocity-pressure coupling in a continuous domain by taking the divergence of the momentum equation (Navier Stokes equation for fluids) and enforcing continuity. The term ∇^2 represents the rate at which the pressure at a given location deviates from the fluid. Thus the pressure Poisson relation provides the rate of

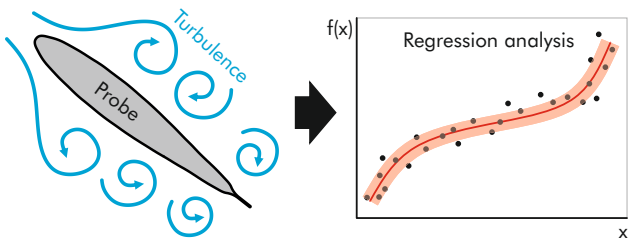

Figure 1: The proposed regression framework for estimating turbulence metrics using a bio-inspired fish-shaped probe.

pressure deviation and is driven by the sum of two source terms; the first term on the right is induced by local gradients in the mean velocity field, and the second source term describes the contribution of the fluctuating velocity components via the Reynolds stresses, including shear and normal components.

The principle difficulty of solving the velocity-pressure coupling lies in the non-linearity of the source terms, compounded by the requirement of using Neumann boundary conditions (which cannot be measured in the field) to solve for the pressure field [3]. The pressure Poisson equation has been solved numerically providing for direct comparison with pressure measurements using high-resolution PIV velocity field data, but due to the complex measurement and numerical analyses, has been limited to physically simple geometric configurations [4].

For measuring turbulence, we adopted a bio-inspired fish-shaped probe which has been applied to estimating the hydrodynamic primitives *bulk flow velocity* and *bulk flow angle* in our previous work [5]. The probe is outfitted with a series of collocated pressure transducers creating an artificial "lateral line probe" (LLP) similar to the biological sensing modality used by fish. The probe simultaneously records the pressure field at 11 different locations at a frequency of 2.5 kHz, and provides pressure data at up to 250 Hz [6], [7]. This is 2.5 times faster than commercially available acoustic probes designed for laboratory use, and is equivalent to the data rates provided by field PIV systems, which due to their complex setup are only able to measure a small range of natural flows. As a result, the fish-shaped sensing array in conjunction with the proposed data processing workflow represent the first artificial lateral line system capable of bulk turbulence measurement.

In this work, we significantly extend the application of the lateral line probe by developing frameworks to estimate bulk turbulence indices which are representative of the higher order, dynamical properties of natural water flows. Classically, high frequency velocity data is used to calculate the fluctuations of the flow field about its time averaged quantity. All previous devices capable of bulk turbulence measurement have first calculated the instantaneous velocity. Our method makes use of a novel data-driven approach which takes advantage of a pressure based system which instead of measuring the velocity at a single point, records the pressure continuously along a fish-shaped body using multiple high-frequency transducers. We then recreated an extreme flow environment in the laboratory using a vertical slot fishway, and record bulk turbulence metric ground truth data using a 3D Vectrino acoustic Doppler velocimeter (25 Hz over 60 seconds interval). Due to the inherent physical complexity of direct turbulence measurement, we have designed a measurement system. In this sense, it allows us to move from a direct measurement problem to a regression problem. which equates to learning a mapping function from a vector-formed feature input to a scalar-valued output. We aim at the least, to match the performance of standard measuring equipment for laboratory studies and then take the device into the field where current standard equipment is difficult or impossible to use. Using a regression based workflow (see Figure 1), it is shown to be the first artificial lateral line sensor system capable of measuring bulk turbulence.

The novelty and contributions of this paper are three-fold:

- This paper is the first work to design a signal processing based framework using a lateral line probe for bulk turbulence metric measurement.
- Instead of using velocity data, we report superior results for regressors against pressure reading deviations that capture high frequency information of flows.
- Experimental results demonstrate good accuracy (11.4%-16.6% proportional mean absolute error of the full measurement scale) accuracy for estimating turbulence metrics in challenging conditions and our regressor is $1.5\times$-$2.0\times$ better than using the mean value over all measurements.

II. Background

A. Existing techniques and limitations for insitu turbulence measurements

Several flow sensing devices capable of delivering turbulence metrics have been developed for laboratory experiments. The most common technologies are particle image velocimetry (PIV) [8] and acoustic Doppler velocimetry (ADV) [9]. Moreover, hot-wire anemometry [10] and laser Doppler velocimetry [11] provide turbulence metrics, but only for lab-scale setups making comparison of natural flows very challenging.

PIV data processing utilizes pattern matching algorithms on images with high particle concentration [12]. Images are divided into small interrogation windows and the movement of particle images is detected typically using cross-correlation of filtered pixel intensities. The result is a spatial (Eulerian) field of velocity vectors on a regular grid whose extent and resolution are determined by predefined interrogation windows. PIV can deliver rapid velocity field estimates, commonly achieving more than 100 Hz and can be used to determine turbulence metrics and their spatial distributions. Field applications of PIV installations are restricted due to the required equipment and are thus limited in scope for insitu measurements [13].

Considering time-averaged velocity field measurements, the ADV has become the most common technology, as commodity devices are straightforward to set-up and operate. Field and laboratory studies using ADV can provide individual measurements of all three velocity components well as the temporal correlation between the directional components. Several commercial ADV devices are available for field measurements in rivers, lakes, and for maritime applications. Considering measurements in rivers, ADV measurements can suffer from limited temporal resolution (typical is 1 Hz for devices in the field) and low signal-to-noise-ratios caused by spike noise, particularly for fast-moving unsteady flows with turbulence and air entrainment [14], [15]. Such conditions are typical in rivers and flows within hydraulic structures.

Compared to PIV and ADV, a bio-inspired fish-shaped probe adopted in this paper is straightforward to apply during field measurement. For the experimental part of this work we selected the popular turbulence metrics [16] listed in Table I.

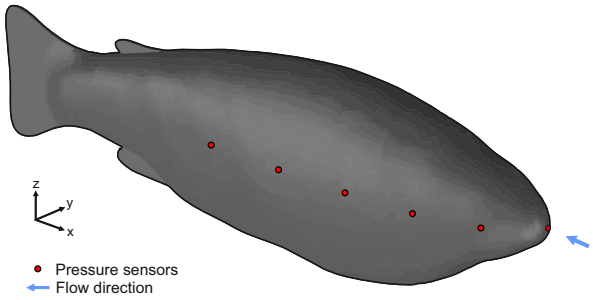

Figure 2: 3D model of the lateral line probe used in this paper. Note that due to the view point only the nose and the right side sensors are visible (red dots).

Table I: Turbulence indices investigated in this work.

Output	*Description*
U	Time-averaged x velocity component (m/s)
V	Time-averaged y velocity component (m/s)
W	Time-averaged z velocity component (m/s)
TKE	Turbulence kinetic energy (m^2/s)
TI_A	Turbulence intensity (unitless)
TI_B	Turbulence intensity, non-normalized (unitless)
TI_C	Turbulence intensity, time-averaged (unitless)
TI_D	Turbullence intensity, non-normalized, time-averaged (unitless)
$REXX$	Reynolds orthogonal stress tensor x (m^2/s^2)
$REYY$	Reynolds orthogonal stress tensor y (m^2/s^2)
$REZZ$	Reynolds orthogonal stress tensor z (m^2/s^2)
$REXY$	Reynolds shear stress tensor xy (m^2/s^2)
$REXZ$	Reynolds shear stress tensor xz (m^2/s^2)
$REYZ$	Reynolds shear stress tensor yz (m^2/s^2)

B. Bio-inspired lateral line probe (LLP)

Our sensor probe is inspired by the lateral line sensing system that has been long recognized as playing a key role in flow sensing capabilities of fishes [17], [18]. The lateral line's unique properties allow for high-fidelity underwater perception and navigation, motivating researchers to construct several artificial organs mimicking the fish lateral line sensing system [19], [20], [21], [22], [23].

The most straightforward implementation is to adopt suitable commercial capacitive, piezoelectic, piezoresistive or magnetic sensors [24]. Our probe is instrumented with multiple piezoresistive sensors located on the sides of a fish-shaped probe body. The piezoresistive sensors measure the strain on a silicon diaphragm whose electrical response is directly proportional to the dynamic pressure experienced by the sensor body. For more details of our sensor and the pressure signals it produces we refer to our previous works focusing on the hardware and low-level signal properties [5], [19], [20]. In particular, our sensor consists of 11 piezoresistive pressure sensors (see Figure 2). The pressure sensors have a resolution of 7.6 Pa / LSB (0.8 mmH20 / LSB) over a 207 kPa span. The signals undergo first and second stage amplification and are digitized independently with a 16-bit analog to digital converter. Temperature estimates via current consumption are made using a shunt resistor. The output signals are $10\times$ oversampled and transmitted over a serial connection at a maximum 250 Hz sample rate.

Owing to growing interest on submersible robotics and ecological characterization of human-made environments the lateral line probes have recently attracted attention. The probes have been demonstrated in laboratory experiments to differentiate between basic flow and turbulence conditions [25], [26], detection of flow regions and probe orientation [27], and a transition metric between steady and unsteady flows [28]. Akanyeti *et al*. [29] demonstrated that the pressure signal response changes according to the physical flow parameters, and De Vries *et al*. [30] estimated flow parameters based on potential flow theory (assuming an ideal, irrotational flow). In our recent work [5], we demonstrated practical measurements of high accuracy for basic flow properties, bulk flow velocity and bulk flow angle, which this work significantly extends to the measurement of dynamical flow parameters in the terms of commonly used turbulence metrics used in flow physics. This paper is based on primitive hydrodynamic features which also have clear physical meaning and are robust to the types of noise and signal distortion expected in natural environments. To the authors' best knowledge our work is the first providing turbulence metrics from lateral line sensor probe signals.

III. Data

A. Experimental setup

In order to investigate the range of hydraulic conditions which more closely match those found in the field, LLP measurements (October 125 Hz, April 250 Hz for 30 seconds) were carried out in a $1:1.6$ scale model of the Vertical Slot Fishway (VSF) installed in Koblenz, Germany. The model consists of three basins with a fixed bed at constant elevation, and adjustable discharge and downstream water surface elevations. Two flow scenarios were investigated: $Q_1 = 0.130$ m^3/s with a mean water depth $h_0 = 0.52$ m and $Q_2 = 0.170$ m^3/s, $h_0 = 0.56$ m. For both flow scenarios the LLP was mounted on Cartesian robot at three reference depths: $0.25h_0$, $0.4h_0$, and $0.6h_0$. At each depth, 24 measurement locations were chosen (Figure 3), providing a planar estimation of the time-averaged velocity magnitude. Point velocity measurements at $0.6h_0$ with an ADV (Vectrino, Nortek) at 25 Hz for 60 seconds are used as the ground truth data. We collected a dataset labelled as "ideal" where all measurement parameters we kept as constant as possible. In order to test the reproducibility of the estimates, another three datasets (labelled "repeatability") were collected where the parameters were kept constant, but representing independent measurements from approximately same conditions. In addition to these four datasets we collected another 8 independent datasets where the probe was disturbed by spatial and angular misalignment. The robustness datasets mimick natural variation that is likely to happen during field studies. The 12 independently acquired datasets are described in Table II.

B. Lateral line signals

The signal received from the probe is 11-dimensional (5 sensors on each side of the probe as shown in Figure 2 and the nose sensor)

$$\boldsymbol{x} = \boldsymbol{x}_{11\times 1} = (x_1, x_2, \ldots, x_{11})^\top \tag{2}$$

where $\boldsymbol{x}$ is the pressure reading at each time step, leading to the full temporal vector $\boldsymbol{x}^t$ sampled at the frequency 250 Hz (see Figure 4). In our previous work [5] we adopted the first and second order

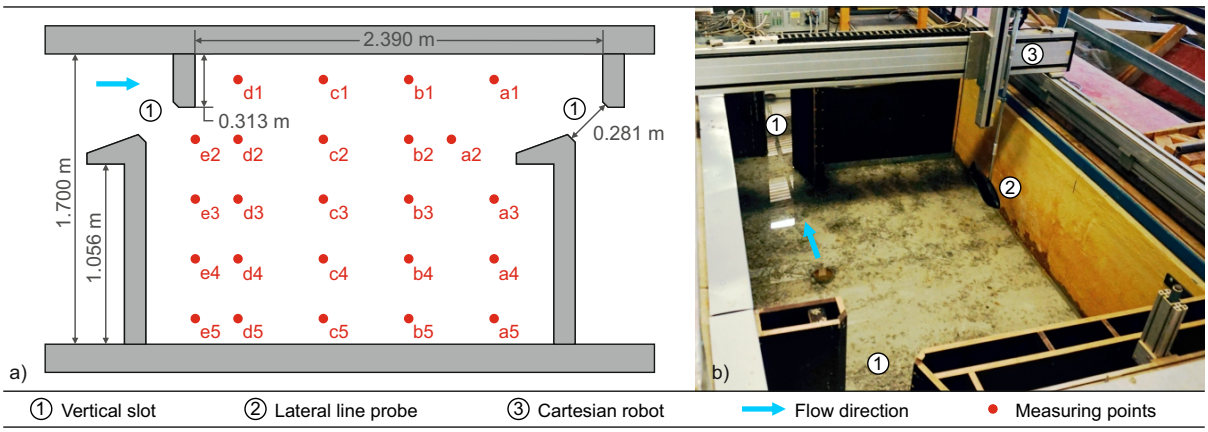

Figure 3: Experimental setup: left diagram shows top view of the experimental environment, along with measurement points (shown in red); right plot illustrates fish pass model and the flow sensing probe mounted on a cartesian (XY) robot.

Table II: Datasets used in the experiments. The repeatability datasets' settings correspond to the same horizontal locations as the ideal case, with varying depth and orientation to mimic variations in the probe position expected in field conditions.

Dataset	*Description*
	- Ideal dataset -
2015-Apr-D1-R1	Q_1, $h_0 = 0.52$ m, $h_r = 0.4h_0$
	- Repeatability datasets -
2014-Oct-D1-R1	Q_1, $h_0 = 0.52$ m, $h_r = 0.4h_0$
2014-Oct-D1-R2	Q_1, $h_0 = 0.52$ m, $h_r = 0.6h_0$
2015-Apr-D5-R1	Q_1, $h_0 = 0.52$ m, $h_r = 0.4h_0$
	- Robustness datasets, for all $h_0 = 0.52$ m, $h_r = 0.4h_0$ -
2015-Apr-D1-R2	Q_1, ± 5 cm lateral probe misalignment
2015-Apr-D1-R3	Q_1, ± 10 cm lateral probe misalignment
2015-Apr-D1-R4	Q_2, $\pm 10^\circ$ angular probe misalignment
2015-Apr-D1-R8	Q_2, $\pm 10^\circ$ angular and ± 5 cm lateral misalignment
2015-Apr-D3-R5	Q_2, $\pm 10^\circ$ angular misalignment
2015-Apr-D3-R6	Q_2, $\pm 20^\circ$ angular misalignment
2015-Apr-D3-R9	Q_2, $\pm 20^\circ$ angular and ± 10 cm lateral misalignment
2015-Apr-D4-R7	Q_2, $\pm 20^\circ$ angular misalignment

moment based features as

$$\boldsymbol{f}_{\text{avg}} = \frac{1}{N}\sum_{n=0}^{N-1} \boldsymbol{x}_n \ , \tag{3}$$

$$\boldsymbol{f}_{\text{std}} = \sqrt{\frac{1}{N-1}\sum_{n=0}^{N-1} (\boldsymbol{x}_n - \boldsymbol{\mu}_f)^2} \ , \tag{4}$$

where N is the number of samples (effect of the sample size is investigated in the experimental section) and $\boldsymbol{\mu}_f$ is the average computed by $\boldsymbol{f}_{\text{avg}}$ or in the case of more robust rank-order statistics

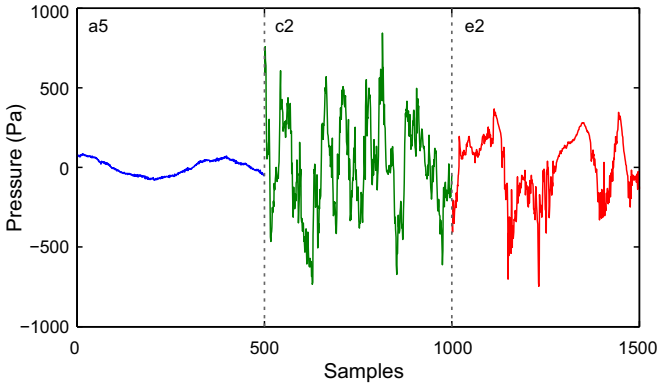

Figure 4: 2 seconds signal (250 Hz) in three different locations (a5, c2 and e2, see Figure 3) of the studied setup.

$\boldsymbol{\mu}_f = \text{median}(\{\boldsymbol{x}\}_N)$. Moreover, in this work we also adopt the frequency domain features used in our preliminary work for flow type classification [31]. This feature is generated by applying the discrete Fourier transformation (FFT) to the input signal and dividing the frequency space to L equally spaced bins for which the total energy is computed. Based on our earlier work we set $L = 100$ which provides fine-grained frequencies and the feature selection is made by the regressor.

IV. Regression Learning

To learn a regression mapping $r^{\mathcal{S}}(\cdot) : \mathcal{X} \rightarrow \mathcal{Z}$, we can train a single-output regression model such as the following popular regression method: Partial Least-Squares (PLS) regression [32]. Partial least square (PLS) regression [32] is employed

here owing to the capability to cope with multicollinearity problem as well as its simplicity in implementation and high computational efficiency, which has recently been applied to a number of signal processing applications [33], [34], [35], [36]. Without generality, as PLS can also cope with multivariate regression problems, *i.e.* . to learn a mapping from a vector-formed input variable to a vector-formed output variable, we will investigate PLS for multivariate regression learning and treat single-variate regression as its special case.

Let us denote that the training set is represented as $\{(\boldsymbol{x}, \boldsymbol{z})\}_i, i = 1, 2, \cdots, \mathrm{M}$. Denote compactly $\boldsymbol{X} = [\boldsymbol{x}_1, \ldots, \boldsymbol{x}_\mathrm{M}]^\top \in \mathbb{R}^{\mathrm{M}\times n}$ and $\boldsymbol{Z} = [\boldsymbol{z}_1, \ldots, \boldsymbol{z}_\mathrm{M}]^\top \in \mathbb{R}^{\mathrm{M}\times l}$. PLS regression can be written as

$$\boldsymbol{X} = \boldsymbol{J}\boldsymbol{P}^\top + \boldsymbol{E}_{\boldsymbol{X}} \tag{5}$$

$$\boldsymbol{Z} = \boldsymbol{K}\boldsymbol{Q}^\top + \boldsymbol{E}_{\boldsymbol{Z}} \tag{6}$$

where $\boldsymbol{J} \in \mathbb{R}^{\mathrm{M}\times d}$ and $\boldsymbol{K} \in \mathbb{R}^{\mathrm{M}\times d}$ are score matrices with d being the number of latent variables, $\boldsymbol{P} \in \mathbb{R}^{n\times d}$ and $\boldsymbol{Q} \in \mathbb{R}^{l\times d}$ are loading matrices, and $\boldsymbol{E}_{\boldsymbol{X}} \in \mathbb{R}^{\mathrm{M}\times n}$ and $\boldsymbol{E}_{\boldsymbol{Z}} \in \mathbb{R}^{\mathrm{M}\times l}$ are the residual matrices. Such a PLS regression projects both input $\boldsymbol{X}$ and target $\boldsymbol{Z}$ into a latent space to maximize the covariance between them, using latent/score vectors. Typical solutions for estimating the score (and loading) matrices are SIMPLS [37] and NIPALS [38]. In this paper, we adopt NIPALS for its better computational complexity (in the order of $O(\mathrm{M}^2)$). With estimated score matrices, the problems (5)-(6) reduce to a typical least squared regression problem

$$\boldsymbol{Z} = \boldsymbol{X}\boldsymbol{L} + \boldsymbol{E}^*, \tag{7}$$

where $\boldsymbol{L} \in \mathbb{R}^{n\times l}$, and $\boldsymbol{E}^*$ is a residual matrix. From [39], $\boldsymbol{L}$ can be computed as

$$\boldsymbol{L} = \boldsymbol{X}^\top\boldsymbol{K}(\boldsymbol{J}^\top\boldsymbol{X}\boldsymbol{X}^\top\boldsymbol{K})^{-1}\boldsymbol{J}^\top\boldsymbol{Z}. \tag{8}$$

Alternatively, other regression models can also be employed such as ridge regression [40] and regression forests [41]. Partial least square regression is adopted owing to its simplicity in implementation and high computational efficiency and several of the existing methods are compared in our experimental part (Section V-D).

V. Experiments

The experiments were conducted using the independent datasets in Table II which all contain measurements from the same 24 spatial locations for which the ground truth turbulence indices were measured by ADV (Section III).

A. Preliminary analysis

There are two practical considerations in analysis of our experimental results: i) the measured turbulence index values are meaningful only in the context of their application. For example the values of turbulence intensity relevant to the study of flows around a bridge pier are several orders of magnitude higher than those impacting a fish's sensory system. In the light, we have elected to compare the performance of the device and proposed regression framework using standard error measures, such as the mean absolute error; and ii) we need to establish a baseline method to compare our results. To address the aforementioned difficulties we propose the following procedures:

- All turbulence measures are normalized to the same scale, $[0, 1]$, which makes errors proportional to the full scale.
- Our baseline is a simple straw man method (SM) that uses the mean value of each turbulence index as an estimate.

Turbulence index normalization
The groundtruth measurements for the spatial locations are given in Table III. We perform the data normalization by:

$$\bar{y}_i = \frac{y_i - \min\{y\}_i}{\max\{y\}_i - \min\{y\}_i} \ . \tag{9}$$

The results of the above normalization are shown in Table IV.

Straw Man Method (SM)
The optimal non-observing decision is the largest mode of each turbulence index value. For simplicity, we assume unimodal distributions and use the normalized turbulence index mean values as the fixed estimate:

$$\begin{aligned}\boldsymbol{y}_{SM} = (&0.34, 0.66, 0.48, 0.36, 0.18, 0.48, 0.71,\\ &0.38, 0.74, 0.65, 0.59, 0.51, 0.50, 0.61)\ .\end{aligned} \tag{10}$$

Using the above SM estimates we computed the estimation errors and the error standard deviations for all turbulence indices. The errors are reported as proportional to the full scale within $[0, 1]$. We report

Table III: Ground truth turbulence index measurements from 24 spatial locations (a1-e5). Note that the turbulence indices TI_A-TI_D are unitless.

	U $[m/s]$	V $[m/s]$	W $[m/s]$	TKE $[m^2/s]$	TI_A $-$	TI_B $-$	TI_C $-$	TI_D $-$	$REXX$ $[m^2/s^2]$	$REYY$ $[m^2/s^2]$	$REZZ$ $[m^2/s^2]$	$REXY$ $[m^2/s^2]$	$REXZ$ $[m^2/s^2]$	$REYZ$ $[m^2/s^2]$
a1	0.26	0.17	0.01	0.05	0.58	0.18	0.39	0.16	-32.00	-37.02	-29.37	-8.10	1.59	1.18
a2	0.59	0.34	0.06	0.07	0.32	0.22	0.32	0.24	-71.29	-43.81	-29.84	-6.81	4.61	2.53
a3	0.28	0.03	-0.01	0.08	0.79	0.23	0.51	0.22	-82.31	-29.31	-41.67	1.34	12.46	5.56
a4	0.09	-0.10	0.02	0.06	1.43	0.20	0.44	0.15	-46.89	-44.93	-31.60	-0.70	6.48	3.64
a5	-0.16	0.01	-0.02	0.04	0.96	0.16	0.40	0.12	-34.11	-20.54	-21.24	-2.15	8.00	-1.26
b1	-0.21	0.09	-0.02	0.06	0.89	0.21	0.37	0.15	-42.63	-51.16	-32.91	-20.93	-3.34	3.43
b2	0.74	0.33	0.08	0.08	0.28	0.22	0.29	0.25	-68.69	-51.96	-30.89	-6.75	-1.64	0.84
b3	0.50	0.13	0.03	0.10	0.51	0.26	0.44	0.27	-115.42	-46.29	-45.40	26.24	15.04	3.85
b4	0.02	0.03	-0.04	0.06	3.69	0.21	0.45	0.15	-54.38	-41.47	-34.03	11.42	11.05	4.19
b5	-0.35	0.01	0.02	0.03	0.39	0.14	0.36	0.14	-27.58	-16.89	-11.82	7.35	4.98	0.03
c1	-0.32	-0.15	0.00	0.04	0.45	0.16	0.40	0.17	-36.37	-19.01	-18.44	-8.38	-3.06	1.37
c2	0.68	0.08	0.03	0.14	0.45	0.31	0.47	0.37	-154.41	-87.35	-39.78	-58.60	-13.71	2.54
c3	0.56	0.05	-0.00	0.13	0.52	0.30	0.39	0.28	-111.81	-92.92	-56.88	55.39	20.27	3.08
c4	-0.06	0.16	-0.02	0.03	0.81	0.14	0.40	0.11	-25.30	-17.96	-15.42	6.56	4.22	-0.27
c5	-0.16	0.08	-0.01	0.02	0.71	0.13	0.38	0.10	-26.40	-11.26	-11.25	-2.08	2.23	0.78
d1	-0.21	-0.11	0.04	0.02	0.48	0.11	0.40	0.11	-16.24	-9.94	-12.34	-3.99	-1.53	-0.56
d2	0.89	-0.11	-0.02	0.15	0.36	0.32	0.39	0.38	-196.69	-56.99	-50.21	-43.54	-0.40	-1.20
d3	0.32	0.00	0.01	0.10	0.82	0.26	0.52	0.26	-86.12	-80.95	-40.84	39.39	13.72	-6.12
d4	-0.14	0.15	0.01	0.03	0.64	0.13	0.34	0.10	-21.31	-19.34	-12.54	-0.96	0.48	0.69
d5	0.04	0.14	0.01	0.02	0.88	0.12	0.49	0.11	-26.67	-9.98	-8.92	-0.10	-0.57	0.29
e2	1.24	-0.54	-0.02	0.04	0.12	0.16	0.10	0.14	-21.72	-36.15	-23.52	-4.18	-0.92	-0.96
e3	-0.07	0.13	0.02	0.01	0.62	0.09	0.44	0.09	-9.07	-8.55	-7.67	2.27	0.65	0.48
e4	-0.09	0.04	0.01	0.01	0.81	0.08	0.39	0.06	-6.78	-5.56	-5.99	-1.66	-0.35	-0.53
e5	0.02	-0.02	-0.06	0.01	0.93	0.06	0.43	0.05	-3.96	-3.55	-3.73	-0.42	-0.87	0.01

Table IV: Normalized ground truth turbulence measurements. Values 0.00 and 1.00 denote the two extremum of the full scale (cf. Table III).

	$\overline{U}$	$\overline{V}$	$\overline{W}$	$\overline{TKE}$	$\overline{TI_A}$	$\overline{TI_B}$	$\overline{TI_C}$	$\overline{TI_D}$	$\overline{REXX}$	$\overline{REYY}$	$\overline{REZZ}$	$\overline{REXY}$	$\overline{REXZ}$	$\overline{REYZ}$
a1	0.38	0.80	0.49	0.30	0.13	0.47	0.69	0.33	0.85	0.63	0.52	0.44	0.45	0.62
a2	0.59	1.00	0.89	0.46	0.06	0.62	0.52	0.57	0.65	0.55	0.51	0.45	0.54	0.74
a3	0.40	0.66	0.35	0.49	0.19	0.64	0.98	0.52	0.59	0.71	0.29	0.53	0.77	1.00
a4	0.28	0.50	0.58	0.38	0.37	0.55	0.81	0.31	0.78	0.54	0.48	0.51	0.59	0.84
a5	0.12	0.63	0.28	0.22	0.24	0.38	0.71	0.21	0.84	0.81	0.67	0.50	0.64	0.42
b1	0.09	0.72	0.30	0.39	0.22	0.56	0.65	0.30	0.80	0.47	0.45	0.33	0.31	0.82
b2	0.68	0.99	1.00	0.48	0.04	0.64	0.45	0.61	0.66	0.46	0.49	0.45	0.36	0.60
b3	0.53	0.76	0.64	0.67	0.11	0.78	0.81	0.68	0.42	0.52	0.22	0.74	0.85	0.85
b4	0.23	0.65	0.11	0.41	1.00	0.57	0.84	0.30	0.74	0.58	0.43	0.61	0.73	0.88
b5	0.00	0.63	0.61	0.15	0.08	0.29	0.63	0.29	0.88	0.85	0.85	0.58	0.55	0.53
⋮	⋮	⋮	⋮	⋮	⋮	⋮	⋮	⋮	⋮	⋮	⋮	⋮	⋮	⋮	⋮

the mean absolute error (MAE) and the standard deviation (STD) values in all experiments. The straw man results are in Table VI (each value is average over all spatial locations, a1-e5).

B. Parameter optimization

For this experiment we selected a single ideal dataset (2015-Apr-D1-R1) and measured the estimation errors using the leave-one-location-out procedure. Based on our preliminary test, we report the results for the parameter combinations with varying sample length (1, 2, 5, 10, 20, 30, 40, 50, 60 seconds) and three types of features including average magnited (avg), standard deviation (std), frequency (fre) investigated in Section III-B for Partial Least-Squares (PLS) regression.

All results are collected to Table V in which results statistically better (F-test of equal variance) than the straw man method (SM) are bolded. The results in Table V indicate that the following turbulence indices can be measured significantly better than the straw man (at least $2\times$ better accuracy): U, TKE, TI_B, TI_D, $REXX$, $REYY$ and $REZZ$. The best overall results were achieved by fixing the sample length to $10s$ and using the *standard deviation* feature. The MAE and STD error values for the selected parameters are given in Table VII.

Using the fixed parameters we computed the

Table V: Mean absolute errors (MAEs) for various parameter settings on the ideal dataset 2015-Apr-D1-R1 (normalized values). Leave-one-location-out protocol and the Partial Least-Square (PLS) regression. The values with statistical significance as compared to the straw man (SM) are emphasized.

	$\overline{U}$	$\overline{V}$	$\overline{W}$	$\overline{TKE}$	$\overline{TI}_A$	$\overline{TI}_B$	$\overline{TI}_C$	$\overline{TI}_D$	$\overline{REXX}$	$\overline{REYY}$	$\overline{REZZ}$	$\overline{REXY}$	$\overline{REXZ}$
SM	0.229	0.135	0.181	0.243	0.105	0.242	0.134	0.230	0.202	0.243	0.254	0.120	0.173
1s-avg	0.145	0.108	0.178	**0.149**	0.178	0.117	0.172	**0.112**	0.218	**0.185**	0.174	0.172	0.203
1s-std	**0.092**	0.127	0.197	0.172	0.181	**0.91**	0.141	0.144	**0.172**	0.191	0.126	0.163	0.153
1s-fre	0.215	0.122	0.176	0.229	0.225	0.103	0.165	0.186	0.233	0.244	**0.121**	0.175	0.154
2s-avg	0.145	0.107	0.173	0.170	0.194	0.134	0.191	**0.114**	0.247	0.212	0.194	0.192	0.225
2s-std	**0.870**	0.126	0.202	**0.158**	0.170	**0.093**	0.146	0.133	**0.164**	**0.182**	0.126	0.156	0.153
2s-fre	0.201	0.121	0.175	0.225	0.222	0.102	0.162	0.179	0.230	0.242	**0.120**	0.174	0.151
5s-avg	0.155	0.090	0.185	0.187	0.216	0.157	0.214	**0.120**	0.251	0.228	0.202	0.210	0.232
5s-std	**0.082**	0.129	0.203	**0.137**	0.152	**0.100**	0.156	**0.121**	**0.158**	**0.163**	0.124	0.144	0.157
5s-fre	0.180	0.114	0.171	0.218	0.219	0.103	0.161	0.172	0.221	0.234	**0.119**	0.171	0.136
10s-avg	0.166	0.101	0.188	0.226	0.254	0.209	0.248	0.152	0.313	0.270	0.237	0.253	0.252
10s-std	**0.083**	0.122	0.204	**0.129**	0.145	0.116	0.173	**0.118**	**0.158**	**0.154**	0.127	0.132	0.167
10s-fre	0.168	0.107	0.177	0.205	0.207	**0.109**	0.163	0.166	0.203	0.222	**0.116**	0.167	0.132
20s-avg	0.178	0.125	0.197	0.249	0.281	0.238	0.281	0.176	0.364	0.286	0.269	0.278	0.248
20s-std	**0.090**	0.127	0.211	**0.132**	0.145	0.136	0.196	**0.119**	**0.175**	**0.161**	0.130	0.126	0.173
20s-fre	0.149	0.101	0.192	0.218	0.216	**0.113**	0.160	0.182	0.202	0.234	**0.108**	0.162	0.127
30s-avg	0.205	0.152	0.200	0.287	0.325	0.272	0.304	0.212	0.397	0.320	0.291	0.295	0.245
30s-std	**0.103**	0.124	0.240	**0.107**	0.153	0.160	0.237	**0.109**	**0.121**	**0.150**	0.125	0.121	0.185
30s-fre	0.151	0.101	0.169	0.231	0.230	**0.132**	0.174	0.207	0.196	0.235	**0.112**	0.172	0.128
40s-avg	0.230	0.158	0.204	0.291	0.329	0.293	0.336	0.220	0.444	0.366	0.290	0.295	0.257
40s-std	**0.103**	0.110	0.249	**0.117**	0.127	0.195	0.253	**0.116**	**0.129**	**0.152**	0.123	0.130	0.204
40s-fre	0.146	0.111	0.196	0.243	0.245	**0.143**	0.177	0.218	0.206	0.257	**0.104**	0.145	0.119
50s-avg	0.234	0.189	0.322	0.327	0.392	0.291	0.312	0.227	0.478	0.369	0.308	0.292	0.318
50s-std	**0.094**	0.125	0.274	**0.161**	0.208	0.202	0.300	**0.164**	**0.169**	**0.207**	**0.084**	0.124	0.234
50s-fre	0.137	0.130	0.212	0.240	0.208	**0.181**	0.210	0.236	0.200	0.246	0.126	0.150	0.155
60s-avg	0.262	0.189	0.236	0.335	0.395	0.341	0.346	0.254	0.457	0.419	0.309	0.326	0.292
60s-std	**0.099**	0.128	0.259	**0.120**	0.198	0.217	0.321	**0.124**	**0.132**	**0.174**	0.118	0.142	0.237
60s-fre	0.132	0.100	0.209	0.258	0.260	**0.185**	0.216	0.240	0.216	0.272	**0.106**	0.183	0.143

Table VI: Normalized estimation errors (MAE: Mean absolute error in $[0, 1]$; STD: Standard Deviation) for the straw man method (SM).

T-index	MAE	STD
$\overline{U}$	0.229	±0.28
$\overline{V}$	0.135	±0.21
$\overline{W}$	0.181	±0.24
$\overline{TKE}$	0.243	±0.30
$\overline{TI}_A$	0.239	±0.30
$\overline{TI}_B$	0.105	±0.20
$\overline{TI}_C$	0.170	±0.26
$\overline{TI}_D$	0.202	±0.26
$\overline{REXX}$	0.243	±0.30
$\overline{REYY}$	0.254	±0.30
$\overline{REZZ}$	0.120	±0.21
$\overline{REXY}$	0.173	±0.22
$\overline{REXZ}$	0.161	±0.22
$\overline{REYZ}$	0.160	±0.22

Table VII: Ideal dataset (2015-apr-D1-R1) estimation errors (normalized) for the best overall parameter settings (10 seconds sample length and the standard deviation feature).

T-index	SM		PLS-10s-std	
	MAE	$\pm STD$	MAE	$\pm STD$
$\overline{U}$	0.229	±0.28	0.083	±0.11
$\overline{TKE}$	0.243	±0.30	0.129	±0.22
$\overline{TI}_B$	0.242	±0.29	0.116	±0.19
$\overline{TI}_D$	0.230	±0.28	0.118	±0.20
$\overline{REXX}$	0.202	±0.26	0.158	±0.23
$\overline{REYY}$	0.243	±0.30	0.154	±0.20
$\overline{REZZ}$	0.254	±0.30	0.127	±0.19

estimates separately for each four ideal datasets and the result points and correlations for the TKE index are shown in Figure 5. The plots indicate that our selected features and the regression perform well in turbulence index estimation, but also reveal a single location for which the estimation systematically fails. The failure for the location $e2$ can be explained by the fact that the probe body takes up

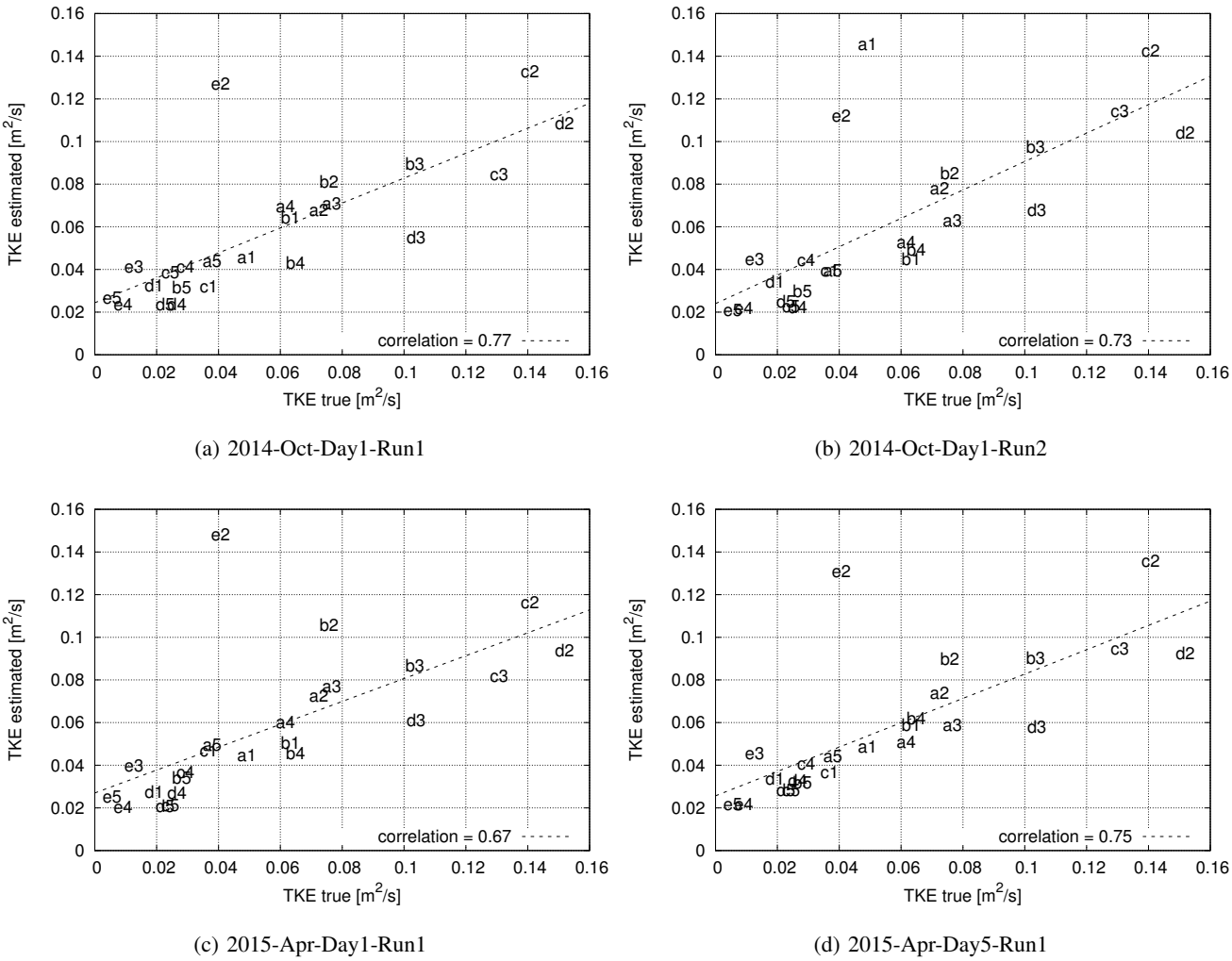

(a) 2014-Oct-Day1-Run1

(b) 2014-Oct-Day1-Run2

(c) 2015-Apr-Day1-Run1

(d) 2015-Apr-Day5-Run1

Figure 5: The correlation plots of the TKE turbulence index for the four repeatability test datasets.

a large portion of the slot opening, thus the flow measurement in the slot is highly disturbed and likely requires a separate regression workflow for turbulence metric comparison. The locations a_1, c_2 and b_2 are in a backwater region upstream of the jet and experience slow, oscillatory water surface fluctuations. This is a possible reason why the total pressure based LLP also shows an outlier for one of the experimental data sets, where longer time-averaging is likely to remove these locations as outliers.

C. Repeatability

The four datasets of constant conditions ("ideal" and "repeatability" in Table II) were used in this experiment. We conducted 4-fold experiments where three datasets were always used in training and one in testing. Moreover, we removed the tested location also from the training data (leave-one-location-out). The results are reported in Table VIII. The accuracies of the turbulence indeces are almost untouched as compared to Table VII indicating that the LLP probe and our regression based estimation provide repeatable estimates of the turbulence indeces.

D. Regression methods

To compare different regression methods, we tested several recent methods: Partial Least Square (PLS) [39], ridge regression (RR) [40], Gaussian Process Regression (GPR) [42], Least Square Support Vector Regression (LSSVR) [43], Random Forests for Regression (RFR) [41] and Support Vector Regression (SVR) [44] There are no significant differences between the four best methods: PLS,

Table VIII: Estimation errors over 4-fold cross-validation using four datasets (the ideal and three repeatability datasets in Table II). The tested location was removed from the regressor training set (leave-one-location-out). The same parameter settings were otherwise used (10 seconds sample length and standard deviation features).

T-index	SM		PLS-10s-std	
	MAE	$\pm STD$	MAE	$\pm STD$
$\overline{U}$	0.229	±0.28	0.085	±0.11
$\overline{TKE}$	0.243	±0.30	0.128	±0.19
$\overline{TI}_B$	0.242	±0.29	0.126	±0.18
$\overline{TI}_D$	0.230	±0.28	0.117	±0.18
$\overline{REXX}$	0.202	±0.26	0.118	±0.20
$\overline{REYY}$	0.243	±0.30	0.138	±0.19
$\overline{REZZ}$	0.254	±0.30	0.153	±0.19

RIDGE, GPRREG and LSSVM in Table IX which indicates that the features are stable and explain well the turbulence indeces. For all other experiments we fixed the regression method to PLS regressor.

Table IX: The previous experiment repeated using various different regression methods.

	T-index			
Regressor	$\overline{U}$	$\overline{TKE}$	$\overline{TI}_B$	$\overline{TI}_D$
SM	0.229±0.28	0.243±0.30	0.242±0.29	0.230±0.28
PLS [39]	0.085±0.11	0.128±0.19	0.126±0.18	0.117±0.18
RR [40]	0.086±0.11	0.126±0.19	0.124±0.18	0.116±0.18
GPR [42]	0.085±0.11	0.126±0.19	0.124±0.18	0.116±0.18
LSSVR [43]	0.085±0.11	0.127±0.19	0.124±0.18	0.116±0.18
RFR [41]	0.071±0.11	0.141±0.22	0.134±0.19	0.126±0.20
SVR [44]	0.084±0.11	0.280±0.29	0.165±0.22	0.153±0.19

E. Robustness

In this experiment the sensor probe was misaligned arbitrarily (spatial location and angle) to mimick more realistic conditions of field measurements (see Table II for details). The ideal datasets were used in training and the 8 misaligned datasets used in testing. The average and worst case errors are given in Table X. The accuracies degrade, but the difference is not significant as compared to the ideal case and therefore our approach can be considered robust to the distortions that are likely to occur in real field measurements.

VI. Conclusions

We proposed a novel combination of a bio-inspired fish-shaped probe of piezoresistive pressure sensors configured similar to a fish's lateral line, standard deviation features computed over 10 second measurement period with the 250Hz sampling frequency, and a robust Partial Least-Square (PLS) regression method to measure hydrodynamical turbulence indeces in realistic conditions. We investigated the effects of various parameters of our approach and verified that it can produce repeatable measurements and is robust to typical variations in field conditions. The mean absolute errors were 8.5%-15.3% for the ideal and 11.4%-16.6% for the challenging data (see Table X) of the full measured scales of each metric (U, TKE, TI_B, TI_D, $REXX$, $REYY$ and $REZZ$) indicating that our probe and regression based signal processing achieve sufficient accuracy for many field measurements. Our regressor was $1.7\times$-$2.7\times$ better than the straw man for the ideal and $1.5\times$-$2.0\times$ for the challenging data. Our system provides an affordable and easy-to-use (no calibration needed) tool for biological field measurements and quantitative hydrodynamic characterization of human-made fish passages and natural environments of fishes.

Table X: Estimation errors for the robustness experiment (8 datasets with probe misalignments used in testing).

	error (MAE)			
	SM	Ideal	Robust.	
T-index			Avg	Worst
$\overline{U}$	0.229	0.085	0.114	0.123
$\overline{TKE}$	0.243	0.128	0.143	0.166
$\overline{TI}_B$	0.242	0.126	0.143	0.170
$\overline{TI}_D$	0.230	0.117	0.130	0.157
$\overline{REXX}$	0.202	0.118	0.130	0.162
$\overline{REYY}$	0.243	0.138	0.158	0.168
$\overline{REZZ}$	0.254	0.153	0.166	0.190

References

[1] H. Tennekes and J. L. Lumley. *A First Course in Turbulence*. MIT Press, 1972.

[2] R. Gurka, A. Liberzon, D. Hefet, D. Rubinstein, and U. Shavit. Computation of Pressure Distribution Using PIV Velocity Data. In *Proceedings of the third PIV Symposium*, 106:1–6, 1999.

[3] P. M. Gresho and R. L. Sani. On pressure boundary conditions for the incompressible Navier-Stokes equations. *International Journal for Numerical Methods in Fluids*, 7(10):1111–1145, 1987.

[4] R. de Kat and B. W. van Oudheusden. Instantaneous planar pressure determination from PIV in turbulent flow. *Experiments in Fluids*, 52(5):1089–1106, 2011.

[5] N. Strokina, J.-K. Kämäräinen, J. A. Tuhtan, J. F. Fuentes-Pérez, and M. Kruusmaa. Joint estimation of bulk flow velocity and angle using a lateral line probe. *IEEE Transactions on Instrumentation and Measurement*, 65(3):601–613, 2016.

[6] J. F. Fuentes-Pérez, J. A. Tuhtan, R. Carbonell-Baeza, M. Musall, G. Toming, N. Muhammad, and M. Kruusmaa. Current velocity estimation using a lateral line probe. *Ecological Engineering*, 85:296–300, 2015.

[7] J. A. Tuhtan, J. F. Fuentes-Pérez, N. Strokina, G. Toming, M. Musall, M. Noack, J.-K. Kämäräinen, and M. Kruusmaa. Design and application of a fish-shaped lateral line probe for flow measurement. *Review of Scientific Instruments*, 87(4):045110, 2016.

[8] S. D. Ponte, S. Malavasi, G. Galzerano, and C. Svelto. Novel particle image velocimetry system based on three-color pulsed lamps and image processing. *IEEE Transactions on Instrumentation and Measurement*, 53(1):175–180, 2004.

[9] B. J. MacVicar, E. Beaulieu, V. Champagne, and A. G. Roy. Measuring water velocity in highly turbulent flows: field tests of an electromagnetic current meter (ECM) and an acoustic Doppler velocimeter (ADV). *Earth Surface Processes and Landforms*, 32:1412–1432, 2007.

[10] P. Ligeza. Use of natural fluctuations of flow parameters for measurement of velocity vector. *IEEE Transactions on Instrumentation and Measurement*, 63(3):633–640, 2014.

[11] L. Simon, O. Richoux, A. Degroot, and L. Lionet. Laser Doppler velocimetry for joint measurements of acoustic and mean flow velocities: LMS-based algorithm and CRB calculation. *IEEE Transactions on Instrumentation and Measurement*, 57(7):1455–1464, 2008.

[12] J. Westerweel. Fundamentals of digital particle image velocimetry. *Measurement Science and Technology*, 8(12):1379–1392, 1997.

[13] L. Bertuccioli, G. I. Roth, J. Katz, and T. R. Osborn. A submersible particle image velocimetry for turbulence measurements in the bottom boundary layer. *Journal of Atmospheric and Oceanic Technology*, 16(11):1635–1646, 1999.

[14] D. E. Dombroski and J. P. Crimaldi. The accuracy of acoustic doppler velocimetry measurements in turbulent boundary layer flows over a smooth bed. *Limnology and Oceanography: Methods*, 5:23 – 33, 2007.

[15] N. Mori, T. Suzuki, and S. Kakuno. Noise of acoustic Doppler velocimeter data in bubbly flows. *Journal of Engineering Mechanics*, 133:122 – 125, 2007.

[16] P. A. Davidson. *Turbulence : An Introduction for Scientists and Engineers: An Introduction for Scientists and Engineers*. Oxford University Press, 2004.

[17] T. Pitcher, B. Partridge, and C. Wardle. A blind fish can school. *Science*, 194(4268):963–965, 1976.

[18] S. M. van Netten and M. J. McHenry. The biophysics of the fish lateral line. In *The Lateral Line System*, pages 99–119. Springer, 2014.

[19] H. E. Daou, T. Salumae, A. Ristolainen, G. Toming, M. Listak, and M. Kruusmaa. A bio-mimetic design and control of a fish-like robot using compliant structures. In *Proceedings of the 15th International Conference on Advanced Robotics (ICAR)*, 563–568, 2011.

[20] A. Qualtieri, F. Rizzi, G. Epifani, A. Ernits, M. Kruusmaa, and M. De Vittorio. Parylene-coated bioinspired artificial hair cell for liquid flow sensing. *Microelectronic Engineering*, 98:516–519, 2012.

[21] N. Izadi and G. J. M. Krijnen. Design and fabrication process for artificial lateral line sensors. In *Frontiers in Sensing: From Biology to Engineering*. Springer Verlag, pages 405–421, 2011.

[22] A. G. P. Kottapalli, M. Asadnia, J. M. Miao, G. Barbastathis, and M. S. Triantafyllou. A flexible liquid crystal polymer mems pressure sensor array for fish-like underwater sensing. *Smart Materials and Structures*, 21(11):115030, 2012.

[23] F. D. Lagor, L. D. DeVries, K. M. Waycho, and D. A. Paley. Bio-inspired flow sensing and control: Autonomous underwater navigation using distributed pressure measurements. In *Proceedings of the 18th International Symposium on Unmanned Untethered Submersible Technology*, 2013.

[24] T. Shizhe. Underwater artificial lateral line flow sensors. *Microsystem Technologies*, 20(12):2123–2136, 2014.

[25] O. Akanyeti, R. Venturelli, F. Visentin, L. Chambers, W. M. Megill, and P. Fiorini. What information do karman streets offer to flow sensing? *Bioinspiration and Biomimetics*, 6(3):1748–3182, 2011.

[26] R. Venturelli, O. Akanyeti, F. Visentin, J. Jezov, L. Chambers, G. Toming, J. Brown, M. Kruusmaa, W. M Megill, and P. Fiorini. Hydrodynamic pressure sensing with an artificial lateral line in steady and unsteady flows. *Bioinspiration and Biomimetics*, 7(3):036004, 2012.

[27] T. Salumäe and M. Kruusmaa. Flow-relative control of an underwater robot. *Proceedings of the Royal Society A*, 469(2153):20120671, 2013.

[28] L. D. Chambers, O. Akanyeti, R. Venturelli, J. Ježov, J. Brown, M. Kruusmaa, P. Fiorini, and W. M. Megill. A fish perspective: detecting flow features while moving using an artificial lateral line in steady and unsteady flow. *Journal of The Royal Society Interface*, 11(99):20140467, 2014.

[29] L. Ristroph, J. C. Liao, and J. Zhang. Lateral line layout correlates with the differential hydrodynamic pressure on swimming fish. *Physical Review Letters*, 114(1):018102, 2015.

[30] L. DeVries, F. D. Lagor, H. Lei, X. Tan, and D. A. Paley. Distributed flow estimation and closed-loop control of an underwater vehicle with a multi-modal artificial lateral line. *Bioinspiration and Biomimetics*, 10(2):025002, 2015.

[31] N. Muhammad, N. Strokina, G. Toming, J. A. Tuhtan, J.-K. Kämäräinen, and M. Kruusmaa. Flow feature extraction for underwater robot localization: preliminary results. In *Proceedings of IEEE International Conference on Robotics and Automation (ICRA)*, pages 1125–1130, 2015.

[32] P. Geladi and B. R. Kowalski. Partial least-squares regression: a tutorial. *Analytica chimica acta*, 185:1–17, 1986.

[33] M. Al Haj, J. Gonzalez, and L. S Davis. On partial least squares in head pose estimation: How to simultaneously deal with misalignment. In *Proceedings of IEEE Conference on Computer Vision and Pattern Recognition (CVPR)*, pages 2602–2609, 2012.

[34] C. C. Loy, K. Chen, S. Gong, and T. Xiang. Crowd counting and profiling: Methodology and evaluation. In *Modeling, Simulation and Visual Analysis of Crowds*, pages 347–382. 2013.

[35] G. Guo and G. Mu. Simultaneous dimensionality reduction and human age estimation via kernel partial least squares regression. In *Proceedings of IEEE Conference on Computer Vision and Pattern Recognition (CVPR)*, pages 657–664, 2011.

[36] K. Chen and Z. Zhang. Learning to classify fine-grained categories with privileged visual-semantic misalignment. *IEEE Transactions on Big Data*, 2016 (in press).

[37] S. De Jong. SIMPLS: an alternative approach to partial least squares regression. *Chemometrics and Intelligent Laboratory Systems*, 18(3):251–263, 1993.

[38] H. Wold. Soft modeling by latent variables: the nonlinear iterative partial least squares approach. *Perspectives in probability and statistics, papers in honour of MS Bartlett*, 1975.

[39] R. Rosipal and L. J. Trejo. Kernel partial least squares regression in reproducing kernel Hilbert space. *The Journal of Machine Learning Research*, 2:97–123, 2002.

[40] K. Chen, S. Gong, T. Xiang, and C. C. Loy. Cumulative attribute space for age and crowd density estimation. In *Proceedings of IEEE Conference on Computer Vision and Pattern Recognition (CVPR)*, pages 2467–2474, 2013.
[41] A. Criminisi and J. Shotton. *Regression Forests*. Advances in Computer Vision and Pattern Recognition. 2013.
[42] F. Perez-Cruz, S. Van Vaerenbergh, J. J. Murillo-Fuentes, M. Lazaro-Gredilla, and I. Santamaria. Gaussian processes for nonlinear signal processing: An overview of recent advances. *IEEE Signal Processing Magazine*, 30(4):40–50, 2013.
[43] J. A. K. Suykens, J. De Brabanter, B. De Moor, and J. Vandewalle. Automatic relevance determination for least squares support vector machine regression. In *Proceedings of International Joint Conference on Neural Networks (IJCNN)*, pages 2416–2421, 2001.
[44] V. Cherkassky and F. M. Mulier. *Support Vector Machines*, pages 404–466. Wiley-IEEE Press, 2007.

Ke Chen received Ph.D major in computer vision under the supervision of Prof. Shaogang Gong and Prof. Tao Xiang at the School of Electronic Engineering and Computer Science, Queen Mary, University of London, UK. He received his B.E. major in automation and M.E. major in software engineering supervised by Prof. Yunong Zhang at the Sun Yat-sen University, China in 2007 and 2009, respectively. Dr. Chen is currently the Academy of Finland post-doctoral research fellow at the Department of Signal Processing, Tampere University of Technology. His research interests include computer vision, pattern recognition, neural dynamic modelling, and robotic inverse kinematics. He has published more than fifty peer-reviewed conference and journal papers in computer vision, neural networks and robotics.

Jeffrey A. Tuhtan completed his B.Sc. in Civil Engineering at the California Polytechnic University, San Luis Obispo in 2004, M.Sc. in Water Resources Engineering and Management in 2007 and Dr.-Eng. degree in hydraulics in 2007 at the University of Stuttgart. He is currently at the Centre for Biorobotics, Tallinn University of Technology where he leads the Environmental Sensing and Intelligence group. His current research interests are applied fluid dynamics, bio-inspired flow sensing and smart devices.

Juan Fran Fuentes-Pérez has been collaborating in several research projects focused on the design, simulation, and evaluation of fishways, and he has been involved in artificial lateral line technology and its applications for the evaluation of aquatic ecosystems and its use in underwater robotics since 2014. He is currently a Junior Researcher with the Centre for Biorobotics, Tallinn University of Technology, Tallinn, Estonia. His current research interests include ecohydraulics, hydraulic modeling, fishways, and underwater robotics.

Gert Toming is currently a Ph.D candidate at the Center of Biorobotics, Tallinn University of Technology, Estonia.

Mark Musall is working at the Institute of Water and River Basin Management, Karlsruhe Institute of Technology, Germany.

Nataliya Strokina received the MSc degrees in Software Engineering and Intelligent Computing from St.Petersburg State Electrotechnical University, Russian Federation and Lappeenranta University of Technology, Finland, correspondingly in 2009.In 2013 she received the PhD degree in Engineering and Technology from Lappeenranta University of Technology. Since 2014 she holds a post-doctoral researcher position at Tampere University of Technology, Finland. Her research interests include machine learning, image understanding, and currently development of the signal processing methods for underwater robotics.

Joni-Kristian Kämäräinen is associate professor of signal processing at the Department of Signal Processing, Tampere University of Technology, Finland. He holds MSc and PhD degrees from Lappeenranta University of Technology in 1999 and 2003, respectively. He leads the Computer Vision Group and his research focuses on 2D and 3D scene analysis, object detection and recognition, signal processing and machine intelligence.

Maarja Kruusmaa is a Head of Centre for Biorobotics in Tallinn University of Technology (Tallinn, Estonia). Her research mainly focuses on bio-inspired underwater robotics. Previously she has worked on flow sensing underwater robots, bio-inspired robot locomotion, experimental fluid dynamics and robot learning.